AIAA JOURNAL
Vol. 31, No. 6, June 1993

Rational Extension of the Clauser Eddy Viscosity Model to Compressible Boundary-Layer Flow

Tibor Kiss* and Joseph A. Schetz†
Virginia Polytechnic Institute and State University, Blacksburg, Virginia 24061

An extension of the Clauser eddy viscosity model for the outer part of a compressible, turbulent boundary layer is proposed. This extension, unlike all of the previous ones, is based on a derivation, and not on ad hoc assumptions. The logic of the derivation of the original model is followed, except that the Crocco integral and the Howarth-Dorodnitsyn transformation are used for the purpose of the comparison with the velocity defect law. Predictions with the new model and two earlier ad hoc extensions of the Clauser model are compared to measured data. Improved predictions are obtained with the new model for both the outer part of the layer and the skin friction coefficient.

Nomenclature

C_M, C_1, C_2	= factors
c_f	= skin friction coefficient
c_p	= specific of heat
F	= velocity defect variable
F^*, F^+, F^{++}	= transformed F-s
g	= Blasius variable
M	= Mach number
m	= see Eq. (17)
T	= temperature
u	= x velocity component
u_τ	= friction velocity
u^*	= Van Driest transformed u
v	= y velocity component
x	= streamwise coordinate
Y	= normal coordinate in the incompressible plane
y	= normal coordinate
δ	= boundary-layer thickness
δ^*	= displacement thickness
δ_k^*	= kinematic displacement thickness
δ_{VD}^*	= displacement thickness calculated from the Van Driest transformed profile
η, η^+, η^{++}	= transformed Blasius coordinates
$\bar{\eta}$	= Blasius coordinate
η_{VD}^*	= η, where $y = \delta_{VD}^*$
μ	= laminar viscosity
μ_T	= eddy viscosity
ρ	= density
τ_w	= wall shear stress
ψ	= compressible stream function

Subscripts

e	= freestream value
w	= wall, actual
0	= wall, pseudolaminar

Introduction

THE Clauser eddy viscosity model[1] for the calculation of the outer part of an incompressible turbulent boundary layer has been successfully used for many years. This model was based on the sound argument that the outer part of a turbulent boundary layer is similar to a pseudolaminar boundary layer with slip velocity at the wall, with the eddy viscosity constant across the outer layer. Comparing calculated pseudolaminar boundary-layer profiles with slip velocity at the wall and the measured velocity defect law for turbulent boundary layers with equilibrium pressure gradients resulted in the well-known formula

$$\mu_T = 0.018 \rho u_e \delta^* \tag{1}$$

Although the Clauser model also has been used for the prediction of compressible boundary layers, its extension for that case has never been done in a systematic manner. Authors usually use the local density for ρ and the incompressible or kinematic displacement thickness δ_k^*, instead of δ^* (Ref. 2). However, for high density variation cases, e.g., with light gas injection, the use of the true displacement thickness δ^* seemed to give better results.[3] In any case, none of these assumptions were based on any theory, and only the fact that they gave satisfactory results in certain cases justified their use.

This paper provides a rational extension of the Clauser model to the compressible case. The fundamental piece of information for the extended model derivation is the observation of Maise and McDonald[4] that the experimental velocity defect law for low Mach number turbulent boundary-layer cases remains valid for high Mach number cases, if first the Van Driest transformation[2] is performed on the velocity profiles. The existence of an experimental velocity defect law then can be exploited in a similar manner as in the original Clauser derivation to predict eddy viscosities. Analogous to that, we need here pseudolaminar, but now compressible, boundary-layer profiles with different slip velocities at the wall. These can be calculated from the Blasius solution[3] with slip velocity using the Crocco integral[3] for the temperature distribution in the boundary layer and applying the Howarth-Dorodnitsyn transformation.[3] In this way, we can obtain a set of profiles for different Mach numbers, each set containing profiles with several slip velocities. Since our goal is to compare these pseudolaminar profiles to the experimental velocity defect law, the Van Driest transformation is applied to the calculated pseudolaminar profiles. Then, with an appropriate coordinate transformation, the different Mach number, different slip velocity profiles can be brought together into a narrow band and compared to the experimental velocity defect law. The result of this comparison is the new extended Clauser model, which in the case of incompressible flows falls back to the original one.

Received Jan. 13, 1992; revision received Sept. 17, 1992; accepted for publication Sept. 17, 1992.

*Graduate Student, Aerospace and Ocean Engineering Department. Member AIAA.

†Professor, Aerospace and Ocean Engineering Department. Fellow AIAA.

Development

The derivation of the extended Clauser model will be carried out according to the outline given in the Introduction. We start out in the same way as Clauser did in the original low speed case derivation. First incompressible, pseudolaminar boundary layers with slip velocities are produced. For the highest generality possible, the viscosity should be allowed to change in the x direction. These profiles can be obtained by solving the well known Blasius differential equation,[3]

$$g''' + g \cdot g'' = 0, \qquad g = g(\bar{\eta}) \tag{2}$$

The boundary conditions, appropriate for the presence of slip velocity, are

$$g'(0) = u_0/u_e \qquad g'(\infty) = 1 \qquad g(0) = 0 \tag{3}$$

Then,

$$u/u_e = g'[\bar{\eta}(Y, x)] \tag{4}$$

where

$$\bar{\eta}(Y, x) = [Y/L(x)] \tag{5}$$

and $L(x)$ is a scaling factor. Our notation is different from that of Clauser,[1] since here y and η are reserved for the compressible profiles; and, also, instead of δ we use L, since we reserve δ for the boundary-layer thickness. The resulting velocity profiles are shown in Fig. 1. These are just the same as the ones Clauser displayed in his original work, except that they are in velocity defect representation.

In the next step, we want to transform these profiles into compressible boundary-layer profiles. The Howarth-Dorodnitsyn transformation[3] can be used, which introduces a distortion of the transverse coordinate in the following way:

$$Y = \int_0^y \frac{\rho}{\rho_e}\,dy \tag{6}$$

If we now apply this transformation, the velocity components can be written as

$$u = \frac{\partial \psi}{\partial Y}, \qquad v = -\frac{\rho_e}{\rho}\left[\frac{\partial \psi}{\partial x} + u\left(\frac{\partial Y}{\partial x}\right)_y\right] \tag{7}$$

Substituting into the steady momentum equation for boundary-layer flow over a flat plate, the resulting equation is obtained as

$$\frac{\partial \psi}{\partial Y}\frac{\partial^2 \psi}{\partial x \partial Y} - \frac{\partial \psi}{\partial x}\frac{\partial^2 \psi}{\partial Y^2} = \frac{\partial}{\partial Y}\left(\frac{\rho\mu}{\rho_e^2}\frac{\partial^2 \psi}{\partial Y^2}\right) \tag{8}$$

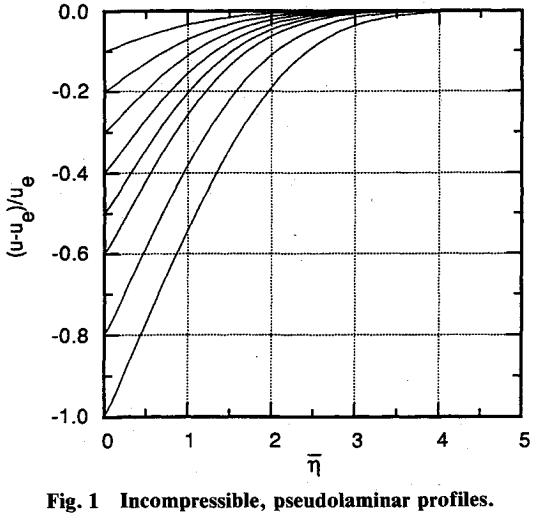

Fig. 1 Incompressible, pseudolaminar profiles.

This equation is very similar to that for constant density, constant property boundary-layer flow and the similarity becomes functional equivalence when $\rho\mu = \text{const}$. Assuming μ to be proportional to T, this condition is satisfied, and we can obtain the compressible boundary-layer profiles by applying the reverse transformation

$$y = \int_0^Y \frac{\rho_e}{\rho}\,dY \tag{9}$$

to the incompressible solution.

However, we have to know the density distribution in the compressible boundary layer to carry out the reverse transformation. For that reason, we need the Crocco integral,[3] which relates the temperature and the velocity in a compressible, adiabatic boundary layer for $Pr = 1$, in the following way:

$$T + \frac{u^2}{2c_p} = T_e + \frac{u_e^2}{2c_p} \tag{10}$$

From this, the ratio of the local to the edge temperature can be expressed in terms of the edge Mach number and the velocity ratio

$$\frac{T}{T_e} = 1 + \frac{\gamma - 1}{2}M_e^2\left[1 - \left(\frac{u}{u_e}\right)^2\right] \tag{11}$$

Since the pressure is constant across a boundary layer,

$$\frac{\rho_e}{\rho} = \frac{T}{T_e} \tag{12}$$

With Eqs. (11) and (12) we obtain ρ_e/ρ as a function of u/u_e. However, u/u_e itself is a function of $\bar{\eta}$ rather than Y [see Eq. (4)], and therefore Eq. (9) has to be rewritten to evaluate it:

$$\frac{y}{L(x)} = \int_0^{\frac{Y}{L(x)}} \frac{\rho_e}{\rho}\left[\frac{Y}{L(x)}\right] d\left[\frac{Y}{L(x)}\right] \tag{13}$$

Now we define η as

$$\eta = [y/L(x)] \tag{14}$$

and Eq. (13) can be rewritten as

$$\eta = \int_0^{\bar{\eta}} \frac{\rho_e}{\rho}(\bar{\eta})\,d\bar{\eta} \tag{13a}$$

The integral has to be carried out numerically, and we obtain a relationship between η and $\bar{\eta}$ in a tabulated form. Next, we can define $F(\eta)$ to represent the velocity defect profiles as

$$F(\eta) = \frac{u(\eta) - u_e}{u_e} = g'[\bar{\eta}(\eta)] - 1 \tag{15}$$

As can be seen from Eq. (11), the transformation is dependent on the edge Mach number, therefore, similar profile sets as in Fig. 1 can be obtained for different edge Mach numbers. A transformed velocity profile set for the case of edge Mach number 4 is shown in Fig. 2.

In the original Clauser derivation for the incompressible case, the next step was to perform an appropriate coordinate transformation to make the profile sets of Fig. 1 fall approximately on the same line to facilitate the direct comparison with the experimental velocity defect law. However, for compressible boundary layers, the velocity defect law is not valid in the same form. As mentioned before, the measured velocity defect profiles do not fall on the same line unless the Van Driest transformation[2] is first performed on them. Therefore, the calculated pseudolaminar, compressible boundary-layer velocity profiles, which we just obtained, have to undergo this transformation too. The Van Driest transformation for the adiabatic case can be written as

$$u^* = (u_e/m^{1/2})\sin^{-1}(m^{1/2}u/u_e) \tag{16}$$

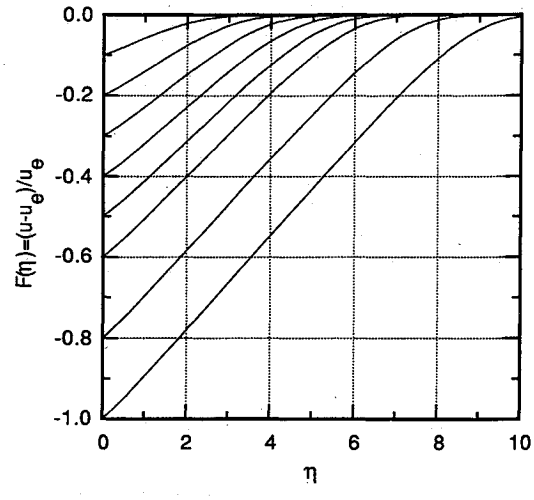

Fig. 2 Pseudolaminar, compressible profiles for $M_e = 4$.

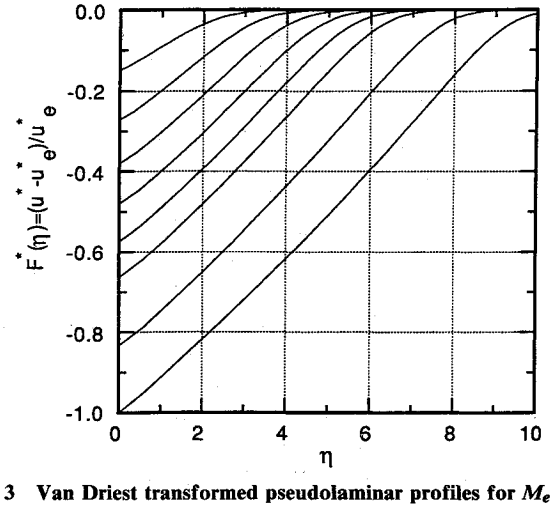

Fig. 3 Van Driest transformed pseudolaminar profiles for $M_e = 4$.

where

$$m = \frac{[(\gamma - 1)/2]M_e^2}{1 + [(\gamma - 1)/2]M_e^2} \tag{17}$$

and u^* is the transformed velocity. It can be seen that in the limit of $M_e \to 0$, $u^* = u$.

Applying the Van Driest transformation on the F function we obtain

$$F^*(\eta) = \frac{u^*(\eta) - u_e^*}{u_e^*} \tag{18}$$

Again, the $M_e = 4$ case is chosen as an example, and the resulting transformed velocity profiles for that case are shown in Fig. 3. It can be seen that the Van Driest transformation did not change the shape of the profiles in Fig. 2 very much. Most changes occurred in the region close to the wall. The Van Driest transformation, however, caused greater changes in the edge velocity, and that is shown in Fig. 4. In fact, the significance of this transformation lies more in its effect on the edge velocity than in its effect on the profile shapes.

Having now obtained pseudolaminar compressible profiles in Van Driest coordinates, we can pick up the logical line followed by Clauser where we left it, and we can develop a coordinate transformation to bring the profiles with different slip velocity and edge Mach number together into a narrow band. The idea is that if the transformation makes the areas above the profiles and the derivatives of the profiles at $y = 0$ the same for all of them then those transformed profiles will be quite close to each other.

The coordinate transformation will be the simplest possible; it will be only a factor on both coordinates F^* and η. The transformed coordinates are

$$F^+ = C_1 \cdot \frac{u^* - u_e^*}{u_e^*} \tag{19}$$

$$\eta^+ = C_2 \cdot \eta \tag{20}$$

and the velocity profiles now are given as $F^+ = F^+(\eta^+)$. Note that C_1 and C_2 are actually functions of u_0 and M_e. The previously mentioned two conditions which will determine C_1 and C_2, can be written now as

$$\int_0^\infty F^+ \mathrm{d}\eta^+ = -1 \tag{21}$$

for the area constraint and

$$\left[\frac{\partial F^+}{\partial \eta^+}\right]_{\eta=0} = 1 \tag{22}$$

for the slope at the wall constraint. These conditions can also be written in terms of F^* and η, with C_1 and C_2 appearing in the formulas

$$C_1 C_2 \int_0^\infty F^* \mathrm{d}\eta = -1 \tag{23}$$

and

$$\frac{C_1}{C_2}\left[\frac{\partial F^*}{\partial \eta}\right]_{\eta=0} = 1 \tag{24}$$

Next, we introduce

$$\delta_{VD}^* = \int_0^\infty \left(1 - \frac{u^*(y)}{u_e^*}\right)\mathrm{d}y \tag{25}$$

i.e., δ_{VD}^* is a displacement thickness for Van Driest transformed profiles. Then, η_{VD}^* can also be introduced as

$$\eta_{VD}^* = \eta(\delta_{VD}^*, x) = \delta_{VD}^*/L(x) \tag{26}$$

that is, η_{VD}^* is the value of η when $y = \delta_{VD}^*$. Incidentally, δ_{VD}^* and η_{VD}^* are the counterparts to δ^* and η_{δ^*} in Clauser's original derivation. If we divide both sides of Eq. (25) by $L(x)$, then with the new notation we can write

$$-\int_0^\infty F^* \mathrm{d}\eta = \frac{\delta_{VD}^*}{L(x)} = \eta_{VD}^* \tag{27}$$

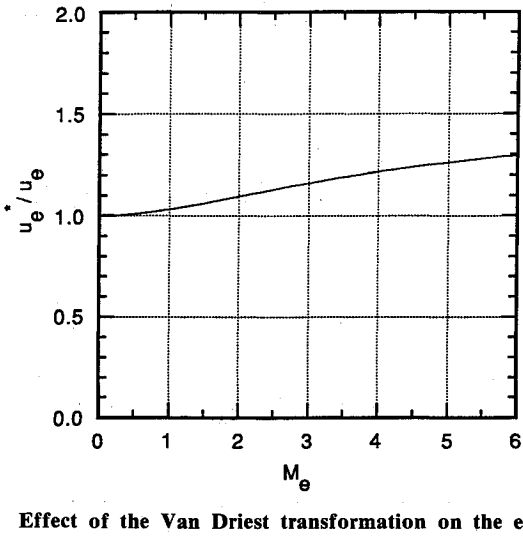

Fig. 4 Effect of the Van Driest transformation on the edge of velocity.

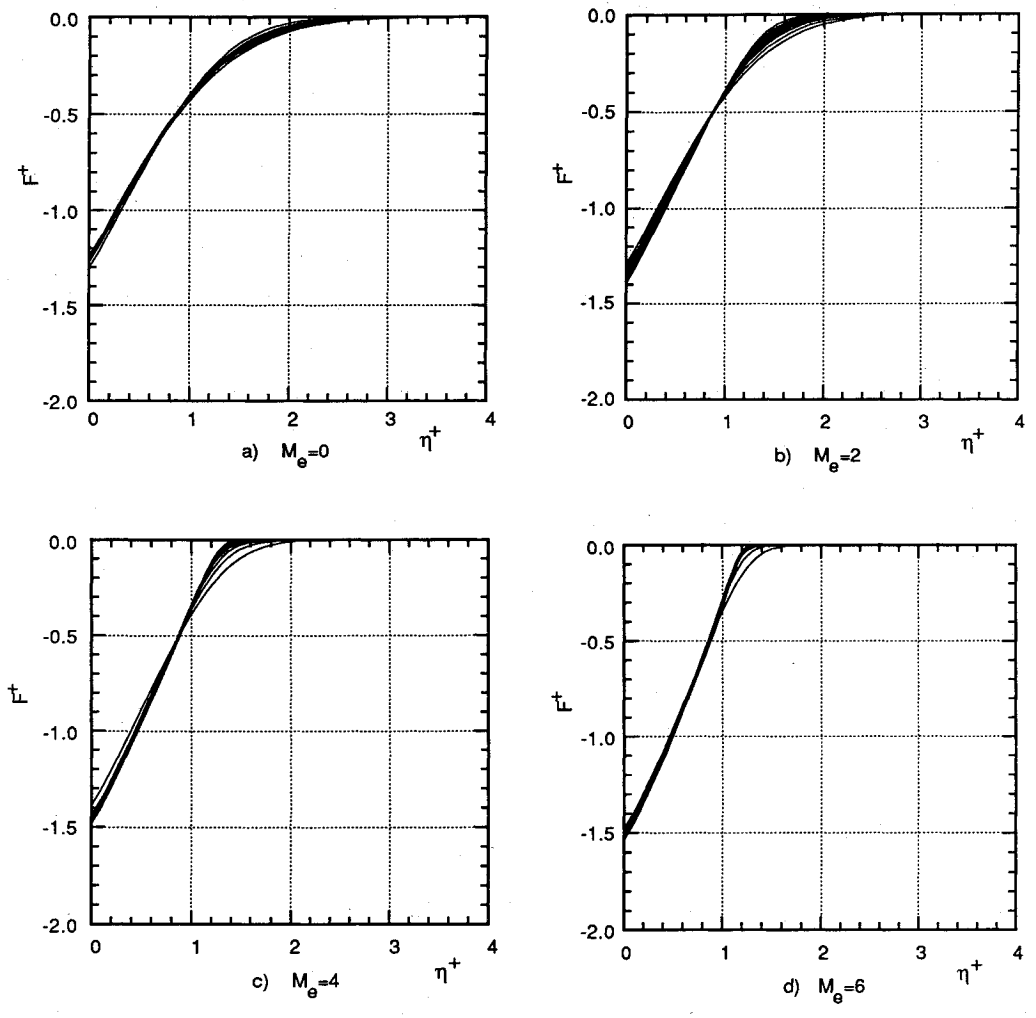

Fig. 5 Defect law-type plots of the transformed pseudolaminar velocity profiles: a) $M_e = 0$, b) $M_e = 2$, c) $M_e = 4$, and d) $M_e = 6$.

Now the solution of Eqs. (23) and (24) for C_1 and C_2 can be written as

$$C_1 = \frac{1}{\sqrt{\left[\frac{\partial F^*}{\partial \eta}\right]_{\eta=0} \cdot \eta^*_{\mathrm{VD}}}} \tag{28}$$

and

$$C_2 = \sqrt{\left[\frac{\partial F^*}{\partial \eta}\right]_{\eta=0} \Big/ \eta^*_{\mathrm{VD}}} \tag{29}$$

Substituting C_1 and C_2 back in Eqs. (19) and (20) we finally obtain

$$F^+ = \frac{u^* - u_e^*}{u_e^* \sqrt{\left[\frac{\partial F^*}{\partial \eta}\right]_{\eta=0} \cdot \eta^*_{\mathrm{VD}}}} \tag{30}$$

and

$$\eta^+ = \eta \sqrt{\left[\frac{\partial F^*}{\partial \eta}\right]_{\eta=0} \Big/ \eta^*_{\mathrm{VD}}} \tag{31}$$

Again, it can be seen that this is the transformed equivalent of the relations obtained by Clauser for the incompressible case.

All of the $F^+ = F^+(\eta^+)$ profiles do not fall in same band. However, if only the same edge Mach number but different slip velocity cases are plotted, they fall in narrow bands as shown in Figs. 5a–5d. An "average" line can be selected for each of the different edge Mach number cases, and these are presented together in Fig. 6. From now on we can work with these average profile lines, since each of them can be considered as a representative of a bigger, constant edge Mach number group. Also, that will mean that the new model will have to incorporate the edge Mach number.

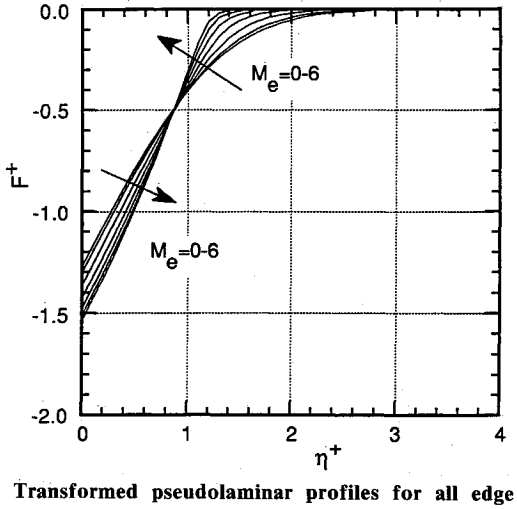

Fig. 6 Transformed pseudolaminar profiles for all edge Mach numbers.

We arrive now at the last coordinate transformation, which will finally make all of the calculated velocity profiles fall on approximately the measured velocity defect law. We introduce F^{++} as

$$F^{++} = C_M F^+ \tag{32}$$

where C_M again is just a transformation factor whose value has to be determined. This factor must be dependent upon the edge Mach number as follows from the previous paragraph, and that is why the M subscript is used. The coordinate η^+ will be transformed into η^{++}; and the condition that the area above the $F^{++} = F^{++}(\eta^{++})$ curves should be the same as the area above the experimental velocity defect law is used. Therefore,

$$\eta^{++} = \frac{1}{C_M} \cdot 3.6\eta^+ \tag{33}$$

is the right choice, since the area above the velocity defect law is 3.6 (Ref. 1). Values for C_M should be given by some simple continuous formula in such a way that the agreement with the experimental velocity defect law is the best possible. The following formula was found to be adequate:

$$C_M = 7.4 - 0.4M_e \tag{34}$$

The resulting transformed pseudolaminar profiles along with the measured velocity defect law are plotted in Fig. 7. The agreement is not quite as good as that for the incompressible model. The lower edge Mach number lines fit the experimental velocity defect law somewhat better than the higher edge Mach number lines. However, the agreement is reasonable overall.

Now we are ready to finally develop the desired eddy viscosity model. The equivalence of the experimental velocity defect law and the calculated profiles can be expressed in the following way:

$$[(u^* - u_e^*)/u_\tau] = F^{++} \tag{35}$$

and

$$y/\delta = \eta^{++} \tag{36}$$

From Eqs. (30), (32), (35) and

$$u_\tau \equiv \sqrt{\frac{\tau_w}{\rho_w}} \tag{36a}$$

(which is the definition of u_τ) we can obtain

$$\tau_w = \frac{1}{C_M^2}\rho_w u_e^{*2}\left[\frac{\partial F^*}{\partial \eta}\right]_{\eta=0}\eta_{\mathrm{VD}}^* \tag{37}$$

However, τ_w can also be expressed as

$$\tau_w = \mu_T|_{y=0}\left[\frac{\partial u}{\partial y}\right]_{y=0} = \mu_T|_{y=0}\left[\frac{\partial F}{\partial \eta}\right]_{y=0}\frac{\eta_{\mathrm{VD}}^*}{\delta_{\mathrm{VD}}^*}u_e \tag{38}$$

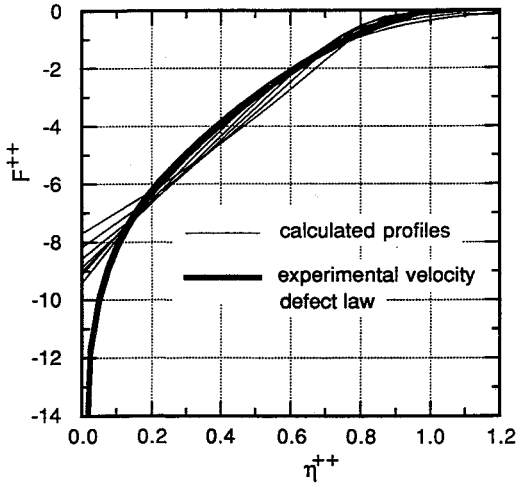

Fig. 7 Transformed pseudolaminar velocity profiles and experimental velocity defect law.

where we used

$$\frac{\partial \eta}{\partial y} = \frac{\eta}{y} = \frac{\eta_{\mathrm{VD}}^*}{\delta_{\mathrm{VD}}^*} \tag{39}$$

following from Eqs. (14) and (26). From Eqs. (37) and (38), μ_T at the wall can be expressed as

$$\mu_T|_{y=0} = \frac{1}{C_M^2}\frac{\left[\dfrac{\partial F^*}{\partial \eta}\right]_{\eta=0}\left(\dfrac{u_e^*}{u_e}\right)}{\left[\dfrac{\partial F}{\partial \eta}\right]_{\eta=0}}\rho_w u_e^* \delta_{\mathrm{VD}}^* \tag{40}$$

The ratio of the derivatives can be written as

$$\left[\frac{\mathrm{d}F^*}{\mathrm{d}F}\right]_{\eta=0} = \left[\frac{\mathrm{d}u^*}{\mathrm{d}u}\right]_{u=u_0}\left(\frac{u_e}{u_e^*}\right) \tag{41}$$

or, with Eq. (16),

$$\left[\frac{\mathrm{d}F^*}{\mathrm{d}F}\right]_{\eta=0} = \left[1 - m\frac{u_0^2}{u_e^2}\right]^{-1/2}\left(\frac{u_e}{u_e^*}\right) \tag{42}$$

where u_0 is the slip velocity of the pseudolaminar boundary layer. Note that u_0/u_e did not appear in Clauser's original derivation. It is introduced here by the use of the Van Driest transformation, and its appearance cannot be avoided. Substituting Eq. (42) into Eq. (40), we obtain the following form for the eddy viscosity on the wall:

$$\mu_T|_{y=0} = \frac{1}{C_M^2}\left[1 - m\frac{u_0^2}{u_e^2}\right]^{-1/2}\rho_w u_e^* \delta_{\mathrm{VD}}^* \tag{43}$$

At this point, we have to point out that the eddy viscosity will have to depend upon the normal coordinate y. It was mentioned earlier that for the Howarth-Dorodnitsyn transformation $\mu \propto T$ had to be assumed. Consequently, the profiles as calculated by Eq. (15) were calculated with $\mu \propto T$. Therefore,

$$\mu_T(y) = \mu_T\left|_{y=0}\frac{T}{T_0} = \mu_T\right|_{y=0}\frac{T}{T_e}\frac{T_e}{T_0} \tag{44}$$

where the temperature ratios can be obtained using Eq. (11).

We have not mentioned yet how u_0/u_e is to be determined. A possible way is the extrapolation of the velocity profile to the wall. The extrapolation has to start out from the outer layer, so one can put a tangent on the velocity profile at, say, $y = \delta/4$, and wherever this tangent intercepts the velocity axis will be u_0. This method is adequate since the pseudolaminar profiles in the inner region are relatively straight.

In summary, for determining the eddy viscosity with the new method, one first finds the edge Mach number; then calculates C_M from Eq. (34); then extrapolates the profiles from $y \sim \delta/4$ to the wall to find u_0/u_e; then calculates T/T_0 from Eq. (11), u_e^* from Eq. (16) and δ_{VD}^* from Eq. (25); and, finally, substitutes all these in

$$\mu_T = \frac{1}{C_M^2}\left[1 - m\frac{u_0^2}{u_e^2}\right]^{-1/2}\frac{T}{T_0}\rho_w u_e^* \delta_{\mathrm{VD}}^* \tag{45}$$

which is our final result, the extended Clauser eddy viscosity model. It is easiest to see how this can work in a computational scheme by considering a simple, explicit "marching" numerical formulation.

The similarity of the original Eq. (1) and the extended model can be easily recognized. Instead of the constant 0.018, in the extended model we have a $u_0(x)/u_e$-dependent expression. Instead of ρ, u_e, and δ^*, now we have ρ_w, u_e^*, and δ_{VD}^*, respectively. The only term which does not correspond to anything in the original model is T/T_0, which is responsible for the y dependence of μ_T.

Furthermore, Eq. (45) has to reduce to Eq. (1) for the case of $M_e = 0$. From Eq. (34), $1/C_M^2 = 0.018$ when $M_e = 0$. From

Eq. (17), $m = 0$ and the magnitude of the square root expression is 1. For incompressible, adiabatic flow $T/T_0 = 1$ and $\rho_w = \rho$. For $M_e = 0$, the Van Driest transformation does not change the velocity as can be seen from Eqs. (16) and (17), so $u_e^* = u_e$. For the same reason $\delta_{VD}^* = \delta^*$. Substituting all of these in Eq. (45), we see that Eq. (1) does result.

The range of flow variables and geometries for which the extended Clauser model is valid needs some discussion. First, there is little information whether the experimental velocity defect law in the form assumed here using the Van Driest transformation holds for edge Mach numbers higher than 6. Next, the pseudolaminar profiles were calculated up to $M_e = 6$ assuming a perfect gas, but it can be debated if that model is truly valid for up to that Mach number. The final conclusion about the validity of the new model for higher Mach numbers must come from comparisons of experimental results and predictions using the new model. Also, an issue is whether the model can be used for nonadiabatic and nonzero pressure gradient cases. The Van Driest transformation used in the derivation here works best for adiabatic cases.[4] Since the original, low speed case model was successfully used for pressure gradient cases (at least for equilibrium pressure gradients), the same might be expected for the new, extended model.

It can be informative to investigate how the eddy viscosities predicted by the new model compare to the predictions by the previously mentioned ad hoc extensions. For the further discussion, the $\mu_T = 0.018\rho(y)u_e\delta^*$ and the $\mu_T = 0.018\rho(y)u_e\delta_k^*$ extensions will be referred to as the δ^* and δ_k^* extensions, respectively. The profiles which will be used for this comparison are the $F = F(\eta)$ [Eq. (15)] pseudolaminar profiles obtained during the derivation of the new model, since they resemble the real, turbulent profiles. Obviously, the relation

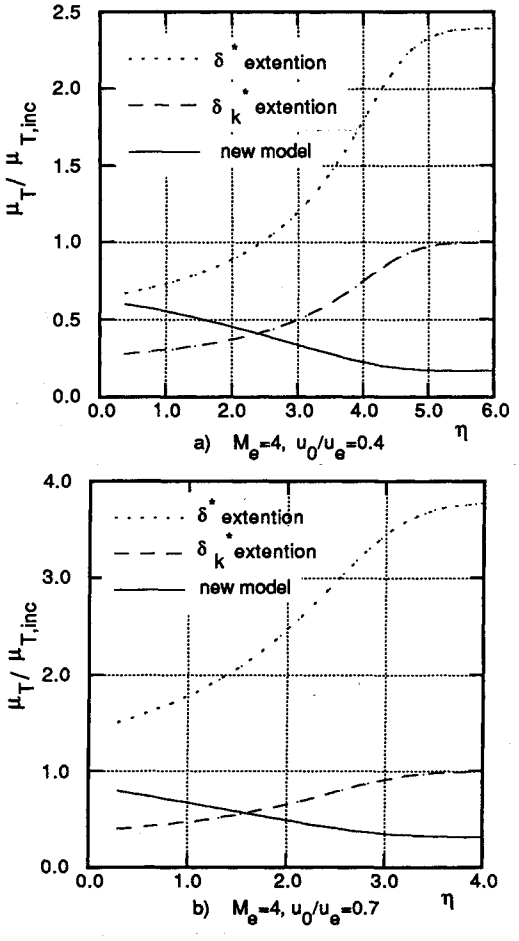

Fig. 8 Normal variation of predicted eddy viscosities: a) $M_e = 4$, $u_0/u_e = 0.4$ and b) $M_e = 4$, $u_0/u_e = 0.7$.

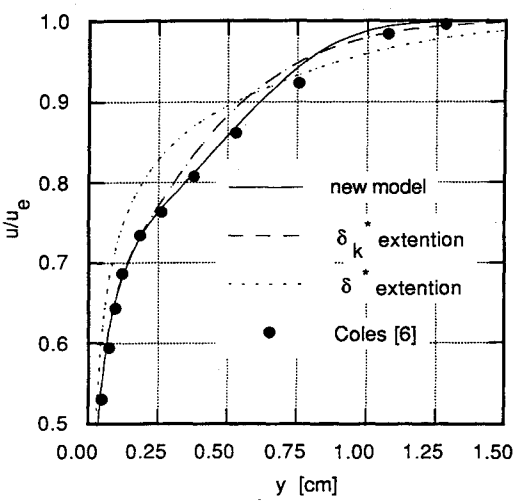

Fig. 9 Calculated and measured velocity profiles for $M_e = 3.7$ experiments of Coles.[6]

between the predictions by the different methods are dependent on the edge Mach number and the slip velocity, since those are the two factors which determine the $F = F(\eta)$ profiles. Conditions of $M_e = 4$ with $u_0/u_e = 0.4$ and 0.7 were chosen as representative. Also, the predictions by the three models were compared to the eddy viscosity that would be obtained by completely neglecting compressibility; i.e., $\mu_{T,inc} = 0.018\rho_e u_e \delta_k^*$. These results are given in Figs. 8a and 8b. It can be seen that toward the edge of the boundary layer the predicted eddy viscosity is growing for the δ^* and the δ_k^* model, and decreasing for the new model. Note, that the Klebanoff factor,[5] which is often used with the ad hoc extensions, would tend to make the predictions by the ad hoc extensions somewhat more like the predictions by the new model by depressing the increase as $y \to \delta$.

Results

The new model was verified by comparing numerical results to measured data. For the numerical results the cell-centered, finite volume formulation of the parabolized Navier-Stokes equations was integrated to the steady-state solution using an implicit factorization method and space marching. The spatial accuracy in the streamwise direction was first order, and in the normal direction it was second order. The eddy viscosity in the outer layer was calculated with three different methods, including the two ad hoc extensions and the new model. The eddy viscosity in the inner layer was always calculated with the well-known Reichardt eddy viscosity model[3]

$$\mu_T = \kappa\mu\left[\left(\frac{\rho y u_\tau}{\mu}\right) - y_a^+ \tanh\left(\frac{\rho y u_\tau}{\mu y_a^+}\right)\right] \tag{46}$$

using the local ρ and μ, as is common practice and $\kappa = 0.41$ and $y_a^+ = 9.7$. It is important to note, that the Klebanoff intermittency factor[5] was not applied in any of the cases. It can be argued, that the pseudolaminar profiles were not calculated with an intermittency factor, and therefore nothing justifies its later introduction.

The first test case is by Coles,[6] who measured the boundary-layer profile and the skin friction over a flat plate in a Mach 3.7 flow. The freestream total pressure and total temperature were 1.4×10^5 Pa and 312 K, respectively. The measurement station was located at 54.6 cm from the leading edge, which is 3.54×10^6 in terms of a Reynolds number. A leading-edge trip was used to cause the boundary layer to be turbulent over the whole length of the plate. The calculated and measured boundary-layer velocity profiles are presented in Fig. 9. It can be seen that the δ^* extension gave the worst result, the δ_k^* extension provided a better result, and the best result was

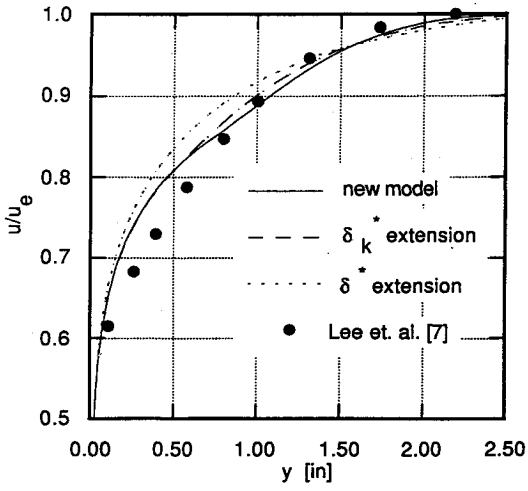

Fig. 10 Calculated and measured velocity profiles for $M_e = 4.86$ experiments of Lee et al.[7]

obtained with the new model. In fact, the agreement with the measurement is quite good for the new model. Also, the skin friction coefficients were calculated. With the δ^* extension $c_f = 0.00193$, with the δ_k^* extension $c_f = 0.00185$, and finally with the new model $c_f = 0.00183$ was obtained. All these predictions are higher than the experimentally obtained 0.00162, but still we can conclude that the prediction obtained by the new model is best.

The second test case by Lee et al.[7] is again a flat plate boundary layer, but the flow in this case is not adiabatic. The edge flow variables are $M_e = 4.857$, $T_e = 72.8$ K and $p_e = 2327$ Pa. The plate is cooled such that the ratio of the wall temperature to the adiabatic wall temperature is 0.74. The boundary layer developed on the wall of a supersonic wind tunnel, so there was no $Re_x = 0$ station to start the calculation from. Therefore, the calculations were carried out between two measurement stations, which were 22 in. apart. The displacement thickness Reynolds number for the entrance station was $Re_{\delta^*} = 2.8 \times 10^5$. Since the first measurement point in the boundary layer was at about $y^+ = 10$, a few points were added to the entrance profile in the $y^+ < 10$ region in such a way that the measured skin friction coefficient was matched. The calculated and measured exit profiles are compared in Fig. 10. Although the new model provides a better profile than the other extensions, the prediction is not quite as good as for the earlier case. An explanation could be that for nonadiabatic boundary layers the Van Driest velocity defect law is not valid as was shown in Ref. 4. The prediction for the skin friction coefficient c_f and the displacement thickness δ^* is much better. For the skin friction coefficient the δ^*, the δ_k^*, and the δ_{VD}^* extensions gave 7.19×10^{-4}, 7.00×10^{-4}, and 7.01×10^{-4}. For the displacement thickness the extensions gave 0.772, 0.742, and 0.753 in., respectively. The measured values for these quantities were $c_f = 7.19 \times 10^{-4}$ and $\delta^* = 0.799$ in.; therefore, it can be concluded that the calculated c_f for all three extensions was basically within the experimental uncertainty, and for the displacement thickness the new model provided the best results.

Conclusions

A new, soundly based extension of the Clauser eddy viscosity model to compressible flow was derived, analyzed, and tested. Although the new model is more complicated than the original one, it is still algebraic and, therefore, is relatively easy to implement compared to models using partial differential equations such as a TKE or Kϵ model.

The new model provides equivalent or better results than the ad hoc extensions for both the velocity profile in the boundary layer and for the skin friction coefficients. The results for the nonadiabatic test case are not as good as for the adiabatic case, as might be expected from the fact that the transformed velocity defect law used in the derivation is not valid for nonadiabatic flow. The applicability of the new model for boundary-layer flows with pressure gradients still has to be investigated in detail. One might assume that the pressure gradient issue will not be critically important, since that was the result in the original, incompressible case. In any event, no simple alternative to the Clauser model exists for nonequilibrium pressure gradients.

References

[1]Clauser, F. H., "The Turbulent Boundary Layer," *Advances in Applied Mechanics,* Vol. IV, Academic, New York, 1956, pp. 1–51.

[2]Cebeci, T., and Smith, A. M. O., *Analysis of Turbulent Boundary Layers,* Academic, New York, 1974, Chaps. 4,5.

[3]Schetz, J. A., *Boundary Layer Analysis,* Prentice-Hall, Englewood Cliffs, NJ, 1993, Chaps. 4,5.

[4]Maise, G., and McDonald, H., "Mixing Length and Kinematic Eddy Viscosity in a Compressible Boundary Layer," *AIAA Journal,* Vol. 6, No. 1, 1968, pp. 73–80.

[5]Klebanoff, P. S., "Characteristics of Turbulence in a Boundary Layer with Zero Pressure Gradient," NACA TN-3178, July 1954.

[6]Coles, D., "Measurements of Turbulent Friction on Smooth Flat Plate in Supersonic Flow," *Journal of the Aeronautical Sciences,* Vol. 21, No. 7, 1954, pp. 433–448.

[7]Lee, R. E., Yanta, W. J., and Leonas, A. C., "Velocity Profile, Skin-Friction Balance and Heat-Transfer Measurements of the Turbulent Boundary Layer at Mach 5 and Zero-Pressure Gradient," Naval Ordnance Lab. Tech. Rept. 69-106, June 1969.